RESEARCH PAPER

Non-isothermal Primary Crystallization Kinetics of the Amorphous $Fe_{85.3}B_{11}P_3Cu_{0.7}$ Alloy

Sima Mirzaei, Hossein Arabi, Hassan Saghafian*, Ali Beitollahi

School of Metallurgy and Materials Engineering, Iran University of Science and Technology (IUST), Tehran, Iran

ARTICLE INFO

ABSTRACT

In the present research, the primary crystallization kinetics of the amorphous $Fe_{85.3}B_{11}P_3Cu_{0.7}$ alloy was analyzed using non-isothermal DSC measurements. The average and local activation energies, E_a, were determined by different isokinetic and isoconversional methods. The results obtained for activation energy in this research, show that due to the complexity of the primary crystallization process in this alloy, isoconversional methods are more suitable than the isokinetic ones. The Avrami exponents lie between about 1 and 2 in a wide temperature range of $370 < T \leq 410°C$. This indicates that one dimensional growth of nuclei with a decreasing rate of nucleation is the main mechanism during non-isothermal primary crystallization process of the amorphous $Fe_{85.3}B_{11}P_3Cu_{0.7}$ alloy which is a new finding for this alloy. Study of magnetic properties in the amorphous and nanocrystalline states revealed that annealing the amorphous ribbons at 440°C for 10 minutes gives rise to a significant increase in saturation magnetization, M_s, i.e. from 144 in as-spun to 201 emu/g in annealed states. This amount of M_s makes this material a good candidate for different applications, especially in transformer cores.

INTRODUCTION

During the last years, Fe-based nanocrystalline materials have attracted much interest for applications in transformer cores, current sensors, magnetic field sensors, filters and so on, due to their excellent soft magnetic properties. These materials are initially produced in amorphous state using rapid solidification methods [1]. Then by annealing the amorphous ribbons nano sized grains within the amorphous matrix can be formed [2].

It has been said [3] that the properties of nanocrystalline alloys are affected by their primary crystallization, thus the crystallization kinetics of these types of alloys is of great importance. Generally, crystallization of the amorphous alloys having the potential to transform to either ultrafine

grains or nanocrystalline structure by annealing, consists of two stages: the first stage usually involves the formation of randomly oriented ultrafine ferromagnetic bcc grains in the amorphous matrix and during the second stage, iron boride compounds such as Fe_2B or Fe_3B phases can be formed resulting to degradation of soft magnetic properties [4]. Thus, in order to obtain proper soft magnetic properties, one should perform a suitable crystallization process at a proper temperature range in order to get a nanocrystalline structure. Also a better understanding of crystallization process of amorphous materials can be achieved by investigating their crystallization kinetics. For this purpose, activation energy, E_a, and parameters such as Avrami exponent, n, which is responsible for the

* Corresponding Author Email: saghafian@iust.ac.ir

crystallization mechanism, should be determined for such materials [3]. There are generally two techniques for studying crystallization kinetics [5]:

1- Isokinetic Methods in which the transformation mechanism and the corresponding kinetic parameters are assumed to be constant throughout the temperature/time range of interest.

2- Isoconversional Methods that are generally used for kinetic studies in non-isothermal conditions. This methods assume that the kinetic parameters can vary with the crystallized fraction, α.

The kinetics of crystallization is mostly analyzed on the base of isokinetic assumptions and isoconversional methods are rarely used for studying crystallization kinetics of amorphous materials [5]. Isokinetic analysis usually results in a single activation energy (average activation energy) which gives an overall picture of the crystallization process [6]. However, the difficulty and uncertainty in the proper kinetic model selection for isokinetic analysis gave rise to development of isoconversional methods which are superior to isokinetic techniques [6].

In the present work, non-isothermal primary crystallization kinetics of Fe$_{85.3}$B$_{11}$P$_3$Cu$_{0.7}$ amorphous ribbons was studied using isokinetic and isoconversional methods for the first time. In addition the effect of primary crystallization on the magnetic properties of the nanocrystalline ribbons has been discussed.

MATERIALS AND METHODS

The alloy ingot with a nominal composition of Fe$_{85.3}$B$_{11}$P$_3$Cu$_{0.7}$ was produced by arc melting method using Fe, B, Cu high purity elements and pre-alloyed Fe$_3$P under a vacuum of ≈10^{-5} mbar.

Then the as-quenched ribbons with a width of 0.6mm and a thickness of 16μm were prepared by single roller melt spinning method working under a high-purity Argon atmosphere (Fig. 1). The rotating copper wheel had a surface velocity of 40 m/s.

The melt-spun ribbons were found to be fully ductile. The initial as-quenched state and the annealed structures were examined by X-ray diffraction (XRD) with Cu Kα radiation. The thermal properties of melt-spun ribbons were evaluated with a differential scanning calorimeter (DSC) working under N$_2$ gas flow at various heating rates of 5, 10, 15 and 20 ˚C/min. Microstructural changes and magnetic properties of the as-spun Fe$_{85.3}$B$_{11}$P$_3$Cu$_{0.7}$ ribbons after annealing the encapsulated ribbons at 440 ˚C for 10 minutes, were studied by X-ray diffraction (XRD) and Vibrating Sample Magnetometer (VSM) at a maximum field of 1.5T. A proper annealing temperature for the ribbons was decided on the
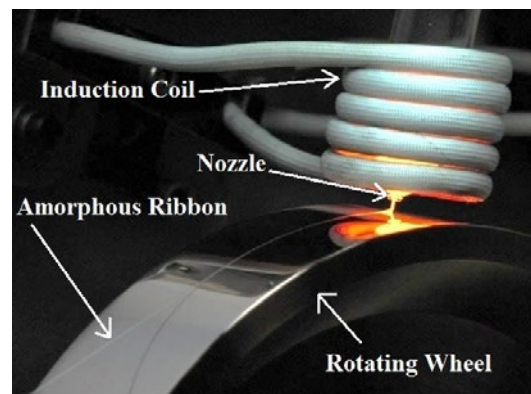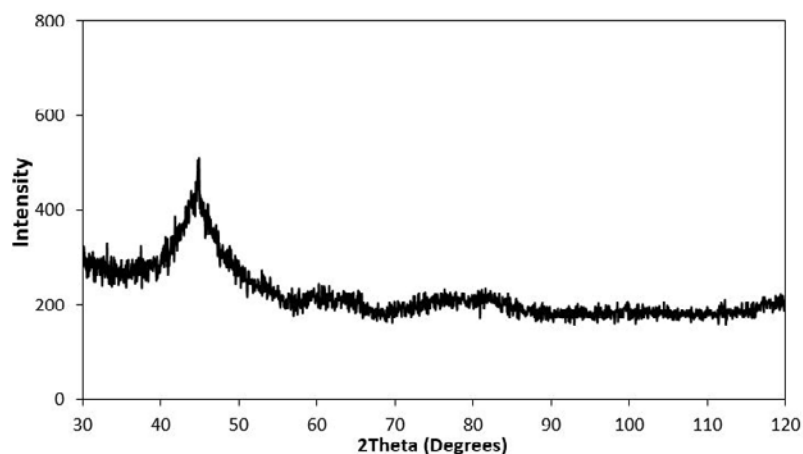

Fig. 1. Melt Spinning Process [7]

Fig. 2. X-ray diffraction pattern from the free surface of as-spun Fe$_{85.3}$B$_{11}$P$_3$Cu$_{0.7}$ ribbon.

base of crystallization temperatures obtained from the DSC curves. Annealing was carried out by putting the encapsulated as-quenched ribbons in a tubular furnace which was already preheated to 440°C.

RESULTS AND DISCUSSION

The X-ray diffraction pattern taken from the free surface (i.e. the surface which was not in touch with quenching wheel) of the rapidly quenched Fe$_{85.3}$B$_{11}$P$_3$Cu$_{0.7}$ ribbon is shown in Fig. 2. The existence of a quasi-amorphous structure could be distinguished from the obtained broad spectrum for this sample presented in Fig. 2.

Crystallization kinetics of the ribbons was studied by non-isothermal differential scanning calorimetry (DSC) technique. Non-isothermal DSC curves of the Fe$_{85.3}$B$_{11}$P$_3$Cu$_{0.7}$ amorphous ribbon at various heating rates of 5, 10, 15 and 20°C/min are presented in Fig. 3. This figure shows that the temperatures of primary and secondary crystallization are well separated.

In addition, the spectra presented in Fig. 3 indicate that with increasing the heating rate from 5 to 20°C/min, the primary and secondary crystallization peak temperatures increased from 371 to 389 °C and 506 to 520 °C, respectively.

Urata et al. [8] reported that the primary and secondary crystallization onset temperatures of amorphous Fe$_{84.8}$B$_8$P$_6$Cu$_{1.2}$ ribbons are 390 and
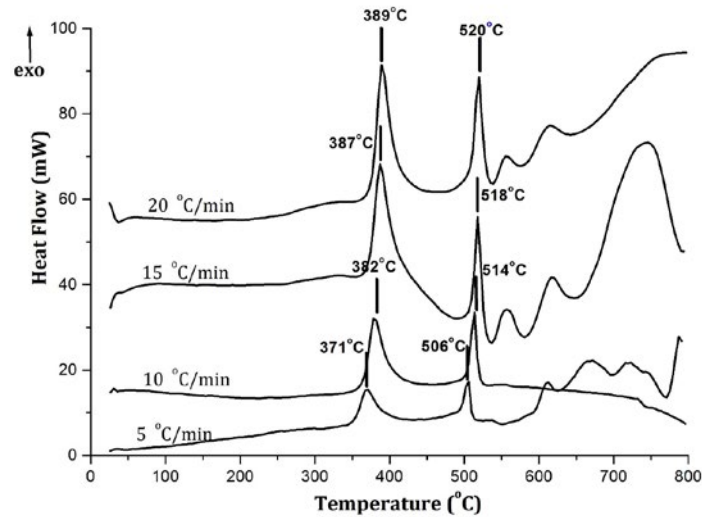

Fig. 3. DSC curves of melt spun Fe$_{85.3}$B$_{11}$P$_3$Cu$_{0.7}$ amorphous ribbons measured at heating rates of 5, 10, 15 and 20 °C/min.
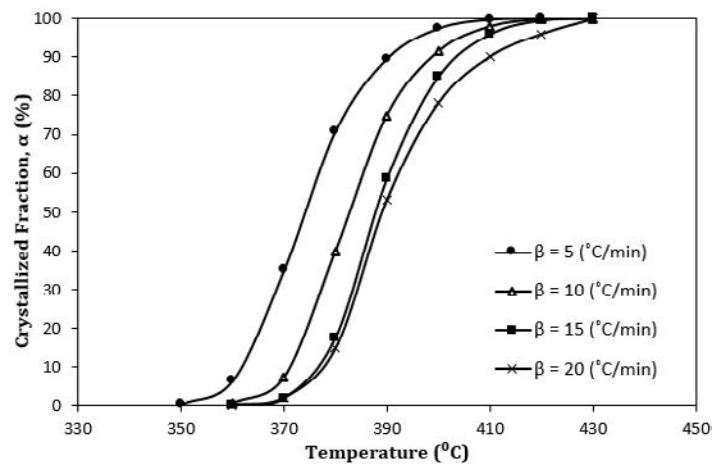

Fig. 4. Variations of crystallized fraction, α, versus temperature for Fe$_{85.3}$B$_{11}$P$_3$Cu$_{0.7}$ ribbons at heating rates of 5, 10, 15 and 20 °C/min.

523°C, respectively; that is in a good agreement with the results obtained in this research. Janotova et al. [9] reported the onset of crystallization temperature for the primary crystallization of Fe$_{81.6}$B$_{14.4}$P$_3$Cu$_1$, Fe$_{80.75}$B$_{14.25}$P$_4$Cu$_1$ and Fe$_{79.9}$B$_{14.1}$P$_5$Cu$_1$ amorphous ribbons are 430, 436 and 447°C, respectively. The comparison of these reported crystallization onset temperatures with those obtained in this work, confirms that increasing the iron content in FeBPCu alloys, shifts the crystallization onset temperatures to lower values and facilitates the formation of α-Fe phase in the amorphous matrix. This can be due to the increase in the formation of iron rich clusters in the as-spun ribbons with increasing iron content.

Crystallized volume fraction (α)

It has been reported [10] that the total magnetostriction, λ$_s$, of nanocrystalline materials can be determined by the Eq. 1:

$$\lambda_s = \upsilon_{cr}\lambda_s^{cr} + \left(1 - \upsilon_{cr}\right)\lambda_s^{amor}$$

Where υ_{cr} denotes the crystallized volume fraction and λ_s^{cr}, λ_s^{amor} are the magnetostriction of ferromagnetic crystallites and amorphous matrix, respectively [10]. Since the magnetostriction of nanocrystalline and amorphous phases are almost constant, variation of crystallized volume fraction could decrease the total saturation magnetostriction of the material. This shows that the soft magnetic properties of nanocrystalline alloys can be improved by proper heat treatment.

Variations of crystallized volume fraction, α, which can be calculated by partial area analysis

according to reference [11], versus temperature for different heating rates are shown in Fig. 4. The curves presented in this figure, have S-shapes containing three different regions. The slow initial part corresponds to the nucleation that occurs at various temperatures for different samples in the bulk of material according to reference [12]. The slope of the initial part of the curves increases gradually up to about 363°C for the heating rate of 5°C/min, indicating that the nucleation rate increased with increasing temperature from 350 to 363°C. The middle sections of these curves indicate the growth of nuclei which already were formed at the initial stages [12]. This stage starts at 363°C and continues up to about 380°C for heating rate of 5°C/min. The constant slope at the middle sections of the curves refers to the constant growth rate of nuclei in this stage. The final part of the S curve which starts at about 380 °C has a descending slope, indicating a decreasing growth rate of crystalline grains within the amorphous matrix during the growth process of the crystalline phase.

Crystallization Activation Energy

Activation energy is defined as the threshold value of energy above which the fluctuation of energy in the activation complex for occurring the elementary reaction is sufficient [3]. In the following sections the values of activation energy required for transformation of amorphous to nanocrystalline structure in Fe$_{85.3}$B$_{11}$P$_3$Cu$_{0.7}$ alloy have been calculated using Kissinger, Ozawa and Augis-Bennett isokinetic methods, as well as
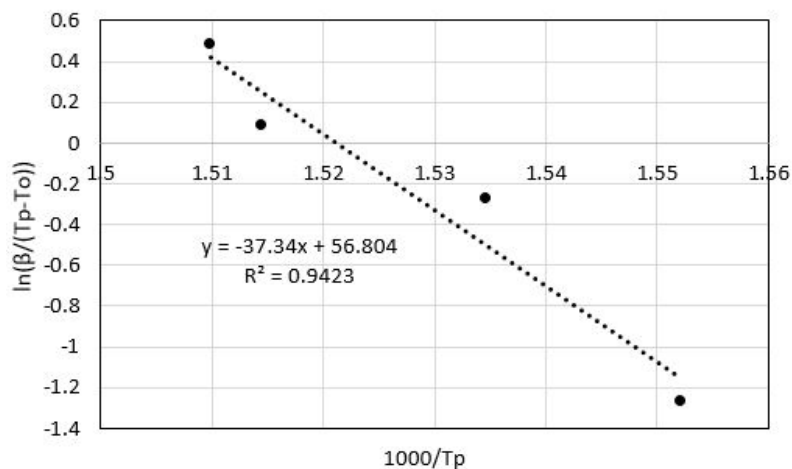

Fig. 5. Variation of Ln(β/T$_p^2$) versus 1000/T$_p$ (Kissinger plot) for different heating rates.

Kissinger-Akahira-Sunose (KAS) and Flynn-Wall-Ozawa (FWO) isoconversional methods. Then the results obtained by these methods were compared with one another.

Isokinetic Methods
Kissinger Method

In the Kissinger method [13], the crystallization activation energy can be obtained from the slope of the plot of $Ln\left(\beta/T_P^2\right)$ vs. $1000/T_P$. Fig. 5 shows the results of Kissinger plot for the present study. On the base of this figure, a single value of E=243kJ/mol was obtained.

Ozawa Method

According to Ozawa [14], the value of activation energy can be obtained from the slope of Ln (β) vs. 1000/T$_p$ plot. This plot for the present study is

shown in Fig. 6. A single value of 254kJ/mol was obtained for the activation energy of crystallization which is almost 5 percent higher than the value obtained by Kissinger method.

Augis and Bennett Method

This method provides the value of activation energy from the slope of Ln [β/(T$_p$-T$_o$)] vs. 1000/T$_p$ plot [15], as shown in Fig. 7 for this study. A single value of 310kJ/mol was obtained for the crystallization activation energy which is almost 27% and 22% higher than the corresponding values obtained from Kissinger and Ozawa methods, respectively.

Isoconversional Methods

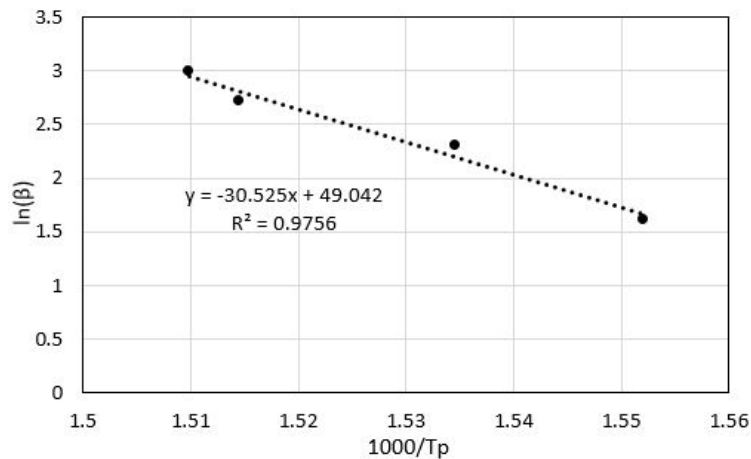In general, the primary crystallization of the amorphous alloys having the potential to transform

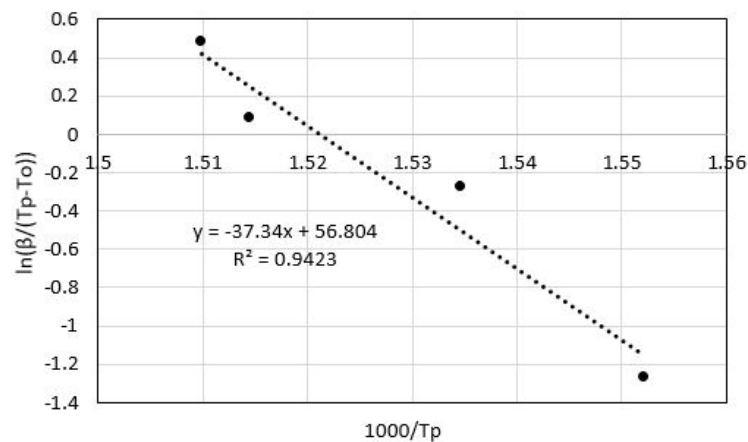Fig. 6. Variation of Ln(β) versus 1000/T$_p$ (Ozawa plot) for different heating rates.

Fig. 7. Variation of Ln(β/T$_p$-T$_o$) versus 1000/T$_p$ for different heating rates.

to nanocrystalline structure is a very complicated process under continuously varied conditions of chemical surrounding as a result of nucleation and growth of nanocrystalline phase [3]. Therefore in order to describe variation in activation energy which presents the changes in nucleation and growth behavior during crystallization process, one should use a local activation energy, $E_a(\alpha)$, which reflects the activation energy when the crystallized volume fraction is α [3].

The isoconversional methods can be classified into two groups: isothermal and non-isothermal methods. Both of these methods are based on the Eq. 2 [5]:

$$\frac{d\alpha}{dt} = k(T)f(\alpha)$$

Where $k(T)$ is the rate constant in the reaction model. Eq. 2 can also be expressed by the Eq. 3 [5]:

$$g(\alpha) = \int_0^\alpha [f(\alpha)]^{-1} d\alpha = \frac{k_0}{\beta} \int_0^T exp\left(-\frac{E_a}{RT}\right)dT$$

The exact solution for the above temperature integral is not available but different approximations have been proposed [5], which

can result to various methods of calculating the activation energy.

Kissinger-Akahira-Sunose (KAS) isoconversional method

In this method, for integrating Eq. 3 one can use the following approximation exp($-y^2$)/y^2 ($y=E/RT$), according to the Murray and White approximation [16]. Using this approximation in Eq. 3 gives rise to the following KAS equation (Eq. 4) [5]:

$$Ln\left(\frac{\beta}{T^2}\right) = Ln\left(\frac{k_0 R}{E_a g(\alpha)}\right) - \frac{E_a}{RT}$$

The plot of Ln(β/T^2) as a function of (1/T) for different crystallized volume fraction, α, gives the slope ($-E_a/R$), which consequently leads to determination of the activation energy for various crystallized volume fraction, $E_a(\alpha)$ [5]. The dependence of activation energy for crystallization of α-Fe phase on crystallized volume fraction, α, is shown in Fig. 8. This figure shows that the local activation energy, $E_a(\alpha)$, increases with increasing the crystallized volume fraction, α. It means that the nanocrystallization process in Fe$_{85.3}$B$_{11}$P$_3$Cu$_{0.7}$ alloy, is a complicated and multi-step process.
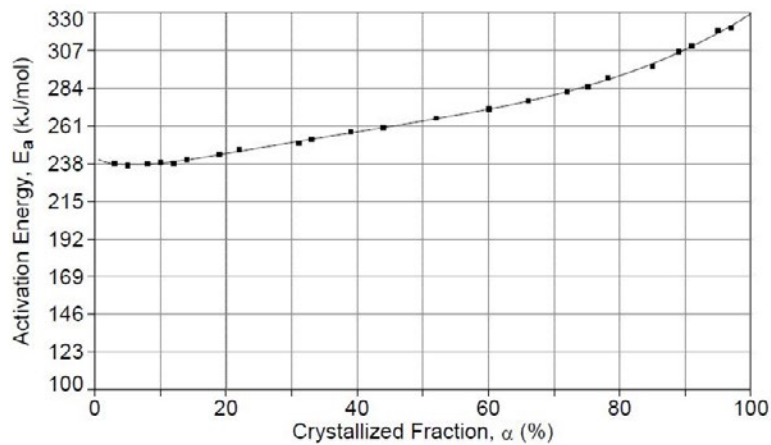

Fig. 8. Dependence of local activation energy, $E_a(\alpha)$, on crystallized volume fraction, α, using KAS method (E_a=242.3568-2.5461α+0.9922α Ln(α)-0.0059$\alpha^{2.5}$+0.00048α^3).

Table 1. The values of crystallization activation energy obtained by different kinetic methods.

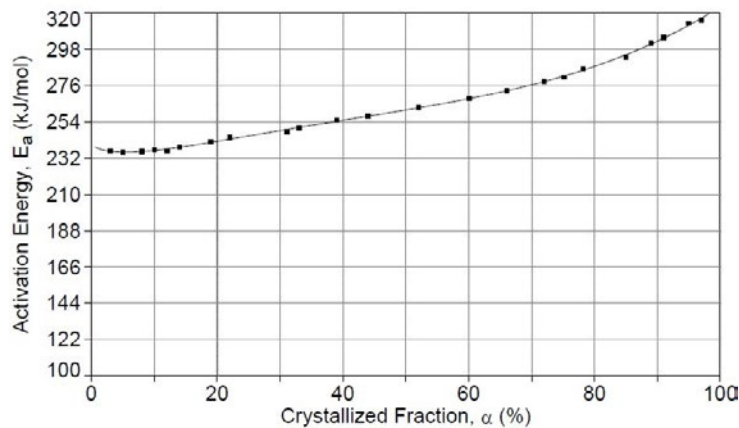| Kinetic Method		Activation Energy (kJ/mol)
Isokinetic Methods	Kissinger	243
	Ozawa	254
	Augis & Bennett	310
Isoconversional Methods	Kissinger-Akahira-Sunose (KAS)	237 -321
	Flynn-Wall-Ozawa (FWO)	235 -316

Fig. 9. Dependence of local activation energy, $E_a(\alpha)$, on crystallized volume fraction, α, using FWO method (E_a=240.4018-2.4088α+0.9431α Ln(α)-0.0057$\alpha^{2.5}$+0.00046α^3).

Flynn-Wall-Ozawa (FWO) isoconversional method

In this method, for integrating Eq. 3 one can substitute the Doyle's approximation into the equation, so that the following equation can be obtained (Eq. 5) [5]:

$$Ln\left(\beta\right)=-1.052\frac{E_a}{RT}+Const.$$

Measuring the slope of Ln (β) vs. (1/T) curves at various crystallized volume fraction, α, leads to determination of local activation energy, $E_a(\alpha)$.

Fig. 9 presents variation of crystallization activation energy, E_a, as a function of crystallized volume fraction, α. This figure indicates that the values of local activation energy obtained by FWO method is in good agreement with those obtained by KAS method.

The results obtained from both KAS and FWO methods, show that the values of crystallization activation energies increase with the crystallized volume fraction, α. Pratap et al. [17] in a similar study, reported that the increase of crystallization activation energy can be due to the increase in energy barrier required for the atoms to diffuse towards the nuclei which can result to crystal growth.

The values of crystallization activation energy obtained by different isokinetic and isoconversional methods for the first crystallization peak are listed in Table 1. The results presented in this table show that any single value for activation energy of $Fe_{85.3}B_{11}P_3Cu_{0.7}$ amorphous alloy in various isokinetic methods, is not reliable, since the value of activation energy can change significantly when using different methods. Comparison of the results obtained for activation energy using different methods in this research indicates that using isoconversional methods provide better understanding of the kinetics of crystallization process for $Fe_{85.3}B_{11}P_3Cu_{0.7}$ alloy.

Calculation of Avrami Exponent

The kinetics of crystallization process in amorphous alloys is mostly described by the JMA equation (Eq. 6) [3]:

$$\alpha=1-exp\left(-\left(kt\right)^n\right)$$

Where n is the Avrami exponent related to the nucleation mechanism as well as growth geometry, k is a rate constant which is a function of temperature related to crystallites nucleation and growth rates [3, 18]. It is said [3] that the Avrami exponent is of great importance in describing the crystallization mechanisms such as nucleation and growth behavior. The value of Avrami exponent, n, can be determined using non-isothermal DSC data and the method proposed by Ozawa [11]. According to this method, the Avrami exponent, n, can be obtained from the plot of log (-Ln (1-α)) vs. log (β) at constant temperature. This plot which appears as a straight line has a slope of –n, α is the crystallized volume fraction at the temperature T and β is the heating rate [11].

The plots of log [-Ln (1-α)] vs. log (β) at different temperatures (360, 370, 380, 390, 400, 410 and 420°C) for the present study are presented in Fig. 10 (a-g).
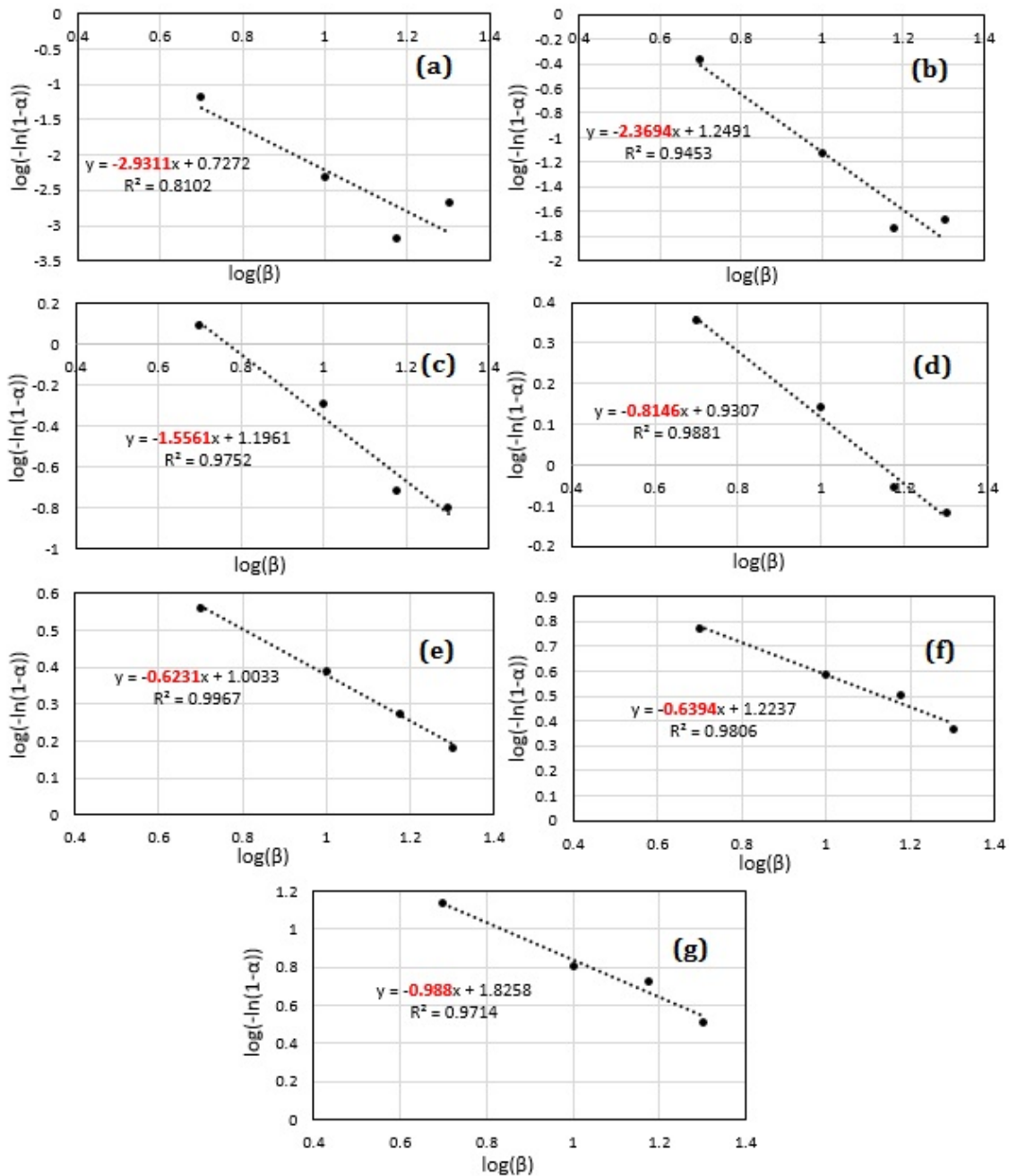
Fig. 10. Variation of Log [-Ln (1-α)] versus log (β) for various temperatures: a) 360°C, b) 370°C, c) 380°C, d) 390°C, e) 400°C, f) 410°C, g) 420°C

The slopes of the lines presented in Fig. 10 (a-g) indicate that the obtained Avrami exponents vary from 0.6 to 2.9 at temperature range 360-420 °C. Variation of Avrami exponent, n, as a function of temperature has been depicted in Fig. 11.

At the beginning of the primary crystallization (i.e. T≤370°C), the calculated Avrami exponent, n, is between 2 and 3. These values of n according to

Lu et al [3] means that two and three dimensional nucleation and grain growth, which are controlled by diffusion, are the dominant mechanisms in this stage. In the middle stage (i.e. 370<T≤410°C), the local Avrami exponents are within the range of 0.6-2. According to Hyatt et al. [19] this shows that in the second stage, one dimensional growth of nuclei with a decreasing rate of nucleation is
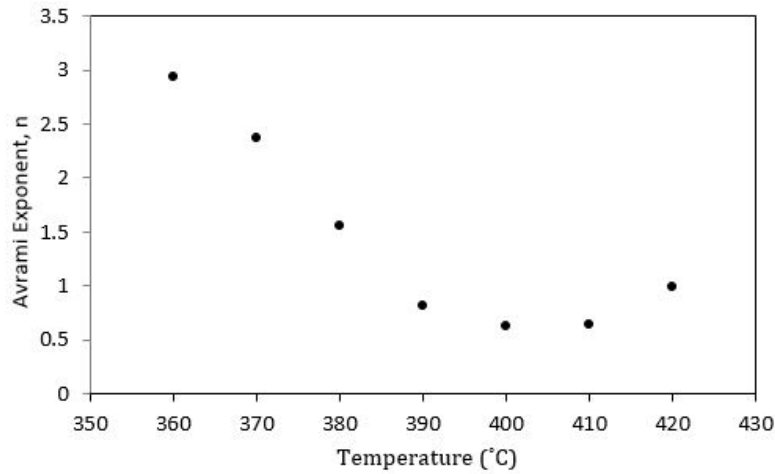
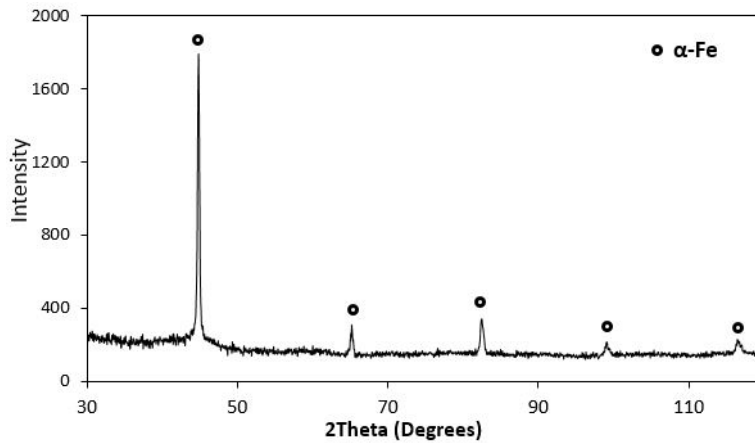Fig. 11. The variations of Avrami exponent, n, with temperature in $Fe_{85.3}B_{11}P_3Cu_{0.7}$ alloy.

Fig. 12. XRD patterns of $Fe_{85.3}B_{11}P_3Cu_{0.7}$ ribbons annealed at 440°C for 10 minutes.

dominant. Thus it seems this kind of nucleation and growth mode is the main mechanism during non-isothermal primary crystallization process. In the final stage (i.e. T>410°C), the n parameter rises to about 1. Sun et al. [20] have pointed out that if inhomogeneous nucleation takes place in the crystallization process and/or inhomogeneously distributed pre-existing nuclei exist in the as-spun ribbons, anomalous Avrami exponent will be expected. So, the inhomogeneous distribution of nuclei in the amorphous ribbons, may be the most important factor in this study which resulted to the widely observed anomalous Avrami exponent as it has been reported by Sun et al. [20]. On the other hand, since the large variation of Avrami exponent with temperature confirms that the crystallization mechanism of $Fe_{85.3}B_{11}P_3Cu_{0.7}$ alloy

is different at various temperature, therefore it seems that isokinetic methods are not suitable for crystallization kinetics study of this alloy.

After studying the kinetic behavior of the alloy, amorphous ribbon was annealed at 440°C for 10 minutes and then its microstructure was studied by XRD technique; the corresponding XRD pattern of this sample is presented in Fig. 12. Formation of ferromagnetic α-Fe phase can be seen in this figure which indicates that transformation of amorphous to nanocrystalline structure, i.e. α-Fe nanocrystals embedded in an amorphous matrix occurred during annealing. The α-Fe crystallite size was estimated by Scherer formula to be about 40nm.

Hysteresis loops of the amorphous and annealed ribbons are shown in Fig. 13. This figure shows annealing of the amorphous ribbons
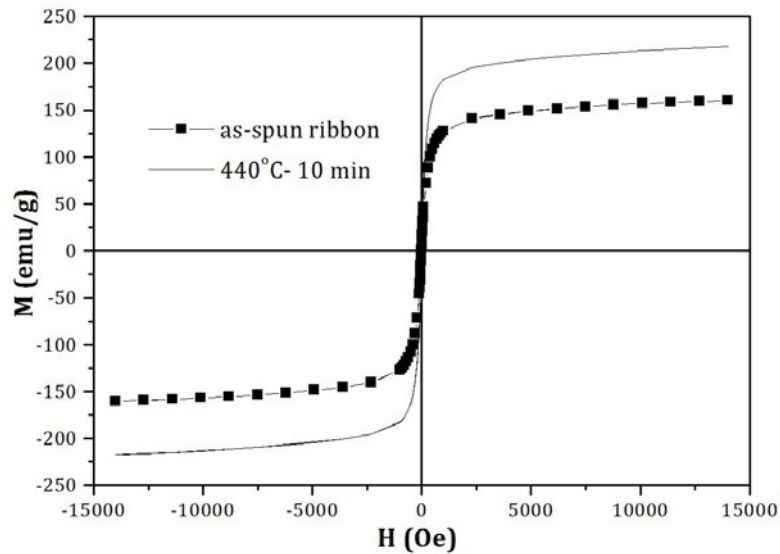
Fig. 13. Hysteresis loops at room temperature for the amorphous and annealed ribbons.

resulted to a significant increase in saturation magnetization, i.e. M$_s$ changed from 144 emu/g in the as-spun state to 201 emu/g in annealed state. The excellent soft magnetic properties obtained in this alloy, make this material a good candidate for different applications, especially in transformer cores.

CONCLUSION

In the present work, the primary crystallization kinetics of the amorphous Fe-rich Fe$_{85.3}$B$_{11}$P$_3$Cu$_{0.7}$ ribbons was studied and the results obtained are summarized below:

1- Activation energies of crystallization were calculated by various methods and compared. The results showed that the nanocrystallization process in Fe$_{85.3}$B$_{11}$P$_3$Cu$_{0.7}$ alloy, is a complicated and multi-step process; and isoconversional methods are much more suitable than the isokinetic methods for determining activation energy of this material.

2- The variation of Avrami exponent, n, as a function of temperature showed that one dimensional growth of nuclei with a decreasing rate of nucleation was the main mechanism during non-isothermal primary crystallization process.

3- Annealing of the amorphous ribbons at 440°C for 10 minutes gives rise to the significant increase in saturation magnetization, M$_s$, i.e. from 144 emu/g in as-spun state to 201 emu/g in annealed state. This indicates that this material is a good candidate for different applications, especially in transformer cores.

CONFLICT OF INTEREST

The authors declare that there are no conflicts of interest regarding the publication of this manuscript.

REFERENCES

1. McHenry M.E, Willard M.A, Laughlin D.E. Amorphous and Nanocrystalline Materials for Applications as Soft Magnets. Prog. Mater Sci, 1999; 44(4):291-433.
2. Shahri F, Beitollahi A, Shabestari S.G, Kamali S. Effects of Heat Treatment on the Structure and Magnetic Properties of Al-Ge Added Fe$_{73.5-x}$Si$_{13.5}$B$_9$Nb$_3$Cu Alloys. Phys Rev B, 2007; 76(2):024434.
3. Lu W, Yan B, Huang W. Complex Primary Crystallization Kinetics of Amorphous Finemet Alloy. J Non-Cryst Solids, 2005; 351(40-42):3320-3324.
4. Herzer G. Nanocrystalline soft magnetic alloys. in: K.H.J. Buschow (Ed.), Handbook of Magnetic Materials, vol. 10, Elsevier, Amsterdam, 1997. p. 415-462.
5. Lad K.N, Savalia R.T, Pratap A, Dey G.K, Banerjee S. Isokinetic and Isoconversional Study of Crystallization Kinetics of a Zr-based Metallic Glass. Thermochim Acta, 2008; 473(1-2):74–80.
6. Pratap A, Patel A.T. Crystallization kinetics of metallic glasses. In: Mastai Y, Advances in crystallization processes. Rijeka, Croatia: InTech; 2012. p. 107-126.
7. Jazayeri Gharehbagh A, Molla J, Esfahani M, Binesh B, Kiani M, Mirzaei S, Arouni H, Bakhtiari R, Parvizi S. Rapid solidification processing and its application in production of amorphous and nanocrystalline materials. 1st ed. Tehran: Sharif Branch of ACECR, 2011 (in Persian).
8. Urata A, Matsumoto H, Yoshida S, Makino A. Fe–B–P–Cu Nanocrystalline Soft Magnetic Alloys with High Bs. J. Alloys Compd.. 2011; 509:S431-S433.
9. Janotová I, Hoško J, Švec P, Janičkovič D, Vlasák G, Švec P. The Study of Magnetically Soft Fe–B–P Based Nanostructures. J Supercond Nov Magn, 2012; 26(4):793-796.

10. Herzer G. Magnetization Process in Nanocrystalline Ferromagnets. Mater Sci Eng, A. 1991; 133:1-5.

11. Grujic S, Blagojevic N, Tosic M, Zivanovic V, Nikolic J. Crystallization Kinetics of $K_2O \cdot TiO_2 \cdot 3GeO_2$ Glass Studied by DTA. Sci Sinter, 2008; 40(3):333-338.

12. Shivaee H, Hosseini H. Advanced Isoconversional Kinetics of Nanocrystallization in $Fe_{73.5}Si_{13.5}B_9Nb_3Cu_1$ alloy. Thermochim Acta, 2009; 494(1-2):80-85.

13. Kissinger H. Reaction Kinetics in Differential Thermal Analysis. Anal Chem, 1957; 29(11):1702-1706.

14. Ozawa T. A New Method of Analyzing Thermogravimetric Data. Bull Chem Soc Jpn, 1965; 38(11):1881-1886.

15. Augis J, Bennett J. Calculation of the Avrami Parameters for Heterogeneous Solid State Reactions Using a Modification of the Kissinger Method. J Therm Anal, 1978; 13(2):283-292.

16. Murray P, White J. Kinetics of the Thermal Decomposition of Clay.4.Interpretation of the Differential Thermal Analysis of Clays. Trans Brit Ceram Soc, 1955; 54:204-237.

17. Pratap A, Kasyap S, Prajapati S.R, Patel A.T. Kinetics of Phase Transformation in Metallic Glasses. ITAS Bull, 2013; 6(1):37-50.

18. Chen H, Wu J, Lin T, Lin J. Crystallization Kinetics in Microphase-Separated Poly(ethylene oxide)-block-poly(1,4-butadiene). Macromolecules, 2001; 34(20):6936-6944.

19. Hyatt M.J, Bansal N.P. Crystallization Kinetics of Barium and Strontium Aluminosilicate Glasses of Feldspar Composition. NASA Technical Memorandum 106624, 1994.

20. Sun N.X, Liu X.D, Lu K. An explanation to the anomalous avrami exponent. Scripta Mater, 1996; 34(8):1201-1207.